### Preparation Method and Industrialization of NbC Ceramic Tujia Jar Tea Roast **Tea Can by High Temperature Sintering**

Wenwen SHI<sup>1</sup>, Zhangli JIN<sup>1\*</sup>, Meng LI<sup>1</sup>, Dongya HU<sup>2</sup>, Fangyu LIU<sup>1</sup>, Yu'e CHEN<sup>1</sup>, Wencheng ZHANG<sup>3</sup>

http://doi.org/10.5755/j02.ms.38648

Received 30 August 2024; accepted 29 January 2025

As a widely loved beverage, tea requires using a roast tea can for roasting and brewing. The selection of materials for the roast tea can itself is crucial for maintaining the tea's freshness and aroma. The study adopts niobium carbide as raw material, introduces nickel alloy and multi-layer graphene, and designs the preparation tools and processes of the materials. This can improve the mechanical and frictional wear properties of the materials used in Tujia jar tea and roasted tea cans, promoting roasted tea cans' industrialization. To enhance the improvement effect of graphene on materials, microwave sintering technology is adopted in this study. Different sintering temperature schemes and multi-layer graphene content schemes are designed. The evaluation and characterization indicators of the mechanical and frictional wear properties of successfully prepared metal ceramic materials are described. The corresponding tools and their properties are clarified. When the sintering temperature was 1440 °C, the bending strength, Vickers hardness, and fracture toughness of the metal ceramic material are the best. When the content of multi-layer graphene was 0.75 wt.%, the material had better mechanical properties and can suppress grain growth. When the multi-layer graphene was 0 wt.%, the corresponding wear amounts of the four hardness on the grinding balls were  $14.4 \times 10^{-6}$ ,  $1.327 \times 10^{-6}$ ,  $1.327 \times 10^{-6}$ , and  $34.59 \times 10^{-6}$  mm<sup>3</sup>/N·m, respectively. These were significantly higher than the wear amount when the multi-layer graphene was 0.75 wt.%. The addition of multi-layer graphene can improve the mechanical and frictional wear properties of materials, reduce wear, and provide material technology support for the industrialization of Tujia jar tea materials.

Keywords: NbC, sintering, roast tea can, multi-layer graphene, Ni, dynamics, friction.

#### 1. INTRODUCTION

According to legend, Shen Nong was the first person to discover and utilize tea. The existence of tea trees can be traced back to 25 million years ago, between the Tertiary and Quaternary periods of the Cenozoic era [1]. Tujia jar tea, as a traditional tea drink with a long history, is mainly distributed in areas such as Hefeng County, Hubei Province, China. The brewing utensils for Tujia jar tea include earthen tea jars, copper or iron cooking pots, etc. The core key processes of brewing are cupping and tea roasting. In addition, the main raw material used for Tujia Roast Tea Can (RTC) is plateau clay, which requires traditional heap firing techniques for high-temperature firing [2]. However, excessive exploitation of plateau clay can easily lead to disasters such as land damage, soil erosion, landslides, and mudslides [3]. Therefore, to promote the industrialization of Tujia jar tea RTC, it should use other materials to replace plateau clay, such as metal ceramics. The commonly used metal ceramics currently include Niobium Carbide (NbC), zirconia, silicon nitride, quartz, tungsten carbide base, and titanium carbide base. The commonly used sintering processes for metal ceramics include pressureless, vacuum hot pressing, discharge plasma, and microwave sintering [4, 5].

Xiong et al. investigated the synergistic relationship between core edge structure and mechanical properties. They prepared four types of metal ceramics containing equimolar amounts, namely tantalum carbide, vanadium carbide, zirconium carbide, and NbC. Vanadium carbide could reduce the lattice mismatch in the distorted region from 4.0 % to 0.8 % [6]. Huang et al. investigated how carbon and tungsten content affected the properties of metal ceramics. Thermodynamics simulation and liquid sintering methods were utilized. Different NbC-Ni based ceramics were prepared by controlling the content of carbon and tungsten. NbC-Ni-based ceramics' mechanical properties were closely related to the phase and NbC grain size [7]. Fernandes et al. investigated the feasibility of using niobium carbide nickel binder cemented carbide as a substitute material. They utilized various ratios of silicon carbide/Ni binders and employed different compaction parameters and sintering conditions. The ratio affected the wear. Sintering conditions were the main factor affecting wear [8].

Daniela et al. selected NbC-Ni metal ceramics and introduced various secondary carbides to design a cutting tool that could replace tungsten carbide. In addition, this study also investigated nickel-based and iron-based adhesives. This material had high hardness, low friction coefficient and wear rate, and excellent performance [9].

<sup>&</sup>lt;sup>1</sup> Hubei Three Gorges Polytechnic, Yichang, 443000, Hubei, China

<sup>&</sup>lt;sup>2</sup> Hubei Longxing Qingjiang Agricultural Science and Technology Development Co., Ltd., Changyang, 443500, Hubei, China

<sup>&</sup>lt;sup>3</sup> Wuhan Business University, Wuhan, 430056, Hubei, China

<sup>\*</sup> Corresponding author: Z. Jin E-mail: jzl@tgc.edu.cn

Liu et al. analyzed the diffusion behavior of four secondary carbides in NbC-Ni-based metal ceramics to explore the microstructural evolution during sintering. They measured the concentration distribution at 1350 °C. The different diffusion behaviors of four types of secondary carbides in NbC-Ni-based metal ceramics further revealed the evolution of NbC grain morphology, etc. [10]. Lin et al. analyzed how NbC affected the properties of titanium nitride carbide-based metal ceramic materials. They utilized liquid-phase sintering to prepare the samples and set different NbC content schemes. When NbC exceeded 12 wt.%, a hard phase having NbC core emerged. With the increase of NbC, this grain size became finer. The metal ceramic's hardness also increased [11]. Tang et al. prepared NbC-10Ni and NbC-12Ni metal ceramics to investigate NbC-Ni metal ceramics' properties prepared by microwave sintering. The sintering temperature significantly affected the microstructure and mechanical properties of NbC-Ni metal ceramics. The dwell time had a relatively small impact. The optimized sintering temperature was 1390 °C and the residence time was 15 minutes [12].

In summary, there is currently abundant research on RTC materials and NbC materials. However, these studies also have certain shortcomings. For example, the brittle defects of NbC materials have not been effectively resolved at present. There is relatively little discussion on NbC materials' friction and wear properties. In addition, the current pressureless sintering methods have difficulties in controlling material sintering. Vacuum pressureless sintering is greatly affected by the process flow, and the productivity of hot-pressing sintering process is low. Based on these issues, to enhance the mechanical and frictional wear properties of Tujia jar tea RTC material and promote its industrialization, NbC-Nickel Alloy (NbC-Ni) material from NbC-based metal ceramics is utilized. Multi-layer Graphene (MLG) is introduced to enhance NbC-Ni's mechanical and frictional wear properties. The research aims to improve RTC materials' mechanical and frictional wear properties, enhance RTC practicality, and promote RTC industrialization. The research innovation is reflected in combining NbC-Ni and MLG. This achieves an improvement in RTC materials' mechanical and frictional wear properties, enhancing RTC quality. This study consists of four parts in total. Firstly, there is a literature review on NbC metal ceramics. Next is the preparation of NbC-Ni/MLG material. Next, the mechanical and frictional wear properties of NbC-Ni/MLG material are analyzed. Finally, there are the conclusions, shortcomings, and prospects of this research.

# 2. PREPARATION OF ROAST TEA CAN MATERIALS AND DESIGN OF PERFORMANCE TESTING METHODS

The Tujia jar tea RTC materials are prepared to improve its mechanical and frictional wear properties. This study selects the raw materials for preparation, explains the equipment required for preparation, and designs the material preparation. To explore how different contents of raw materials affect the sintering temperature and the properties of the prepared materials, different experimental schemes are designed. Finally, to analyze the prepared materials'

properties, the evaluation indicators and characterization methods for material properties are explained.

#### 2.1. Preparation of NbC-Ni/MLG metal ceramics

The study utilizes NbC-Ni material from NbC-based metal ceramics and introduced MLG to enhance the mechanical and frictional properties of NbC-Ni material. This is beneficial for preparing RTC materials that are more resistant to friction and wear, improving the mechanical properties of RTC materials, and promoting the industrialization of Tujia jar tea. MLG is utilized to replace Ni in the matrix. NbC has the advantages of strong chemical stability, and resistance to high-temperature softening, adhesion, and wear, which has extensive application in aerospace and equipment manufacturing [13]. However, NbC-based metal ceramics are relatively brittle. The mechanical and wear resistance properties of NbC-Ni metal ceramic materials still need further improvement. Graphene has excellent mechanical and frictional wear properties, which has significant advantages in improving NbC-Ni metal ceramic materials' performance. To prepare NbC-Ni/MLG materials, NbC, Ni, and MLG powders are utilized as raw materials. Table 1 presents information on different raw materials.

Table 1. Information on different raw materials

Material	Source	Average particle size	Purity	Density
NbC	Shanghai Hanlang New Material Technology Co., Ltd	1.0 μm	≥99.9 %	7.80 g/cm <sup>3</sup>
Ni	Shanghai Yanbei New Materials Technology Co., Ltd	0.5 ~ 3.5 μm	≥99.9 %	9.01 g/cm <sup>3</sup>
MLG	Source	Layer diameter	Thickness	Number of layers
	Shanghai Fuqi Industry and Trade Co., Ltd	4 ~ 60 μm	3.2 ~ 8.2 nm	6 ~ 11

From Table 1, NbC and Ni powders have a purity of over 99.9 %, densities of 7.80 g/cm³ and 9.01 g/cm³, respectively, and average particle sizes of 1.0  $\mu m$  and 0.5 – 3.5  $\mu m$ , respectively. Meanwhile, in the NbC-Ni metal-ceramic structure, the volume percentages of NbC and Ni are 88 % and 12 %, the weights are 86.4 % and 13.6 %, and the molar percentages are 80 % and 20 %, respectively. In addition, MLG powder has layer diameters, thicknesses, and layers of 4 – 60  $\mu m$ , 3.2 – 8.2 nm, and 6 – 11 layers, respectively. This study also adopts other equipment to prepare NbC-Ni/MLG materials, including QM-1SP planetary ball mill, WDW-100E universal material mechanics testing machine, MW-L0316HV vacuum microwave sintering furnace, etc.

To analyze how different contents of MLG affect NbC-Ni materials, five different MLG contents are set, namely 0, 0.25, 0.5, 0.75, and 1 wt.%. This study names these five MLG contents A1, A2, A3, A4, and A5, respectively. To prepare NbC-Ni/MLG, microwave sintering technology is

adopted. This process can perform rapid heating, reduce sintering temperature, refine material structure, and improve material properties. This process is energy-saving, efficient, safe, pollution-free, and highly controllable [14]. The experiment analyzes how different sintering temperatures affect NbC-Ni/MLG's mechanical properties. In terms of sintering temperature, heating rate, and holding time, the study referred to experimental setups from similar studies [15]. Therefore, the study sets up four different sintering temperature experiments, namely 1380 °C, 1400 °C, 1440 °C, and 1460 °C, which are named as B1, B2, B3, and B4, respectively. In addition, the heating rate for sintering is 16-26 °C/min, and the holding time is 16 minutes. Fig. 1 shows the preparation of NbC-Ni/MLG metal ceramics.

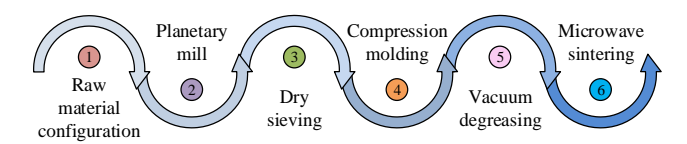


Fig. 1. Preparation process of NbC-Ni/MLG metal ceramics

From Fig. 1, the preparation of NbC-Ni/MLG metal ceramics involves six steps, including raw material preparation, planetary ball milling, drying and screening, compression molding, vacuum degreasing, and microwave sintering. The raw material configuration involves the design of raw material components, namely the use of NbC, Ni, and MLG powders. When performing planetary ball milling, it should add molding agents, dispersants, and anhydrous ethanol. After one day of ball milling at a speed of 300 r/min, the raw materials should be thoroughly dispersed and mixed. The temperature for drying and sieving needs to be controlled at 70 °C. A 200 mesh sieve is required for sieving. Compression molding requires maintaining a pressure of 250 MPa for 2 minutes. Vacuum degreasing requires heating the sample to 550 °C and holding it for 1 hour before removing impurities from the sample. There are four different temperatures for microwave sintering, but they all need to be kept warm for 15 minutes after sintering.

## 2.2. Design of performance testing and characterization methods for NbC-Ni/MLG metal ceramics

Experiments are designed to analyze the prepared NbC-Ni/MLG metal ceramics' mechanical and frictional properties. The mechanical and frictional properties' characterization methods are explained. To conduct friction and wear tests, the TIME M5112 reciprocating friction and wear testing machine is utilized. This testing machine is mainly used for reciprocating friction and wear tests of different solid materials under different conditions. The diameter of the test ball is 6 mm, the high-frequency oscillation frequency range is  $10-200\,\mathrm{Hz}$ , and the temperature control accuracy is as high as  $0.1\,^{\circ}\mathrm{C}$ . This instrument has good accuracy and reliability.

The study fixes the sample block on the stage and placed the grinding ball on the sample block, followed by reciprocating friction. In addition, this study selects four different hardness grinding balls. They are 304 stainless steel, 45 steel, GCr15 steel, the representative of high

carbon chromium bearing steel, and YG6 hard alloy of tungsten cobalt materials. The corresponding hardness values are 200 HV, 240 HV, 772 – 832 HV, and 1500 HV, respectively. To ensure experimental accuracy, the temperature is controlled at  $21 \pm 4^{\circ}$ C. In addition, the sample is polished, and the surface roughness is reduced to  $\leq 0.1~\mu m$ . The processed samples and grinding balls need to be cleaned and dried before testing. During the experiment, the friction duration is set to 52 minutes, the additional load is 68 N, and the back-and-forth friction distance is 6 mm.

To analyze NbC-Ni/MLG metal ceramics' mechanical properties, indicators such as Vickers hardness, etc. are selected. Phase analysis, graphene structure verification, and Thermo Gravimetric Analysis-Differential Scanning Calorimetry (TG-DSC) are conducted. For phase analysis, an X-Ray Diffraction (XRD) diffractometer is adopted, with measurement speeds and ranges of 3°/min and 11 ~ 91°, respectively. For the verification of graphene structure, a Raman spectrometer is utilized. The laser wavelength is 532 mm. In addition, to analyze NbC-Ni/MLG metal ceramics' friction and wear properties, the study explains them through the friction coefficient and wear rate. The solution for Vickers hardness *HV* is represented by Eq. 1 [16]:

$$HV = 1.8544 \times \frac{P}{d^2},\tag{1}$$

where P is the experimental load; d refers to two diagonal lines' average length of the pressure mark. The solution for fracture toughness  $K_{IC}$  is represented by Eq. 2

[17]: 
$$K_{IC} = 8.89 \times 10^{-2} \times \sqrt{\frac{HV \cdot P}{4\overline{b}}}$$
, (2)

where  $\bar{b}$  is the pressure mark's average crack length. The bending strength  $\delta$  is represented by Eq. 3 [18]:

$$\delta = \frac{3DT}{2ah^2},\tag{3}$$

where D is the material's ultimate strength; T is the span; a is the sample width; h is the sample thickness. The wear rate  $\omega$  is represented by Eq. 4 [19]:

$$\omega = \frac{R}{FL} = \frac{QY}{FL},\tag{4}$$

where R is the wear volume; F is the applied load; L is the total frictional sliding distance; Q is cross-sectional area of the abrasion mark; Y is the amplitude of back-and-forth movement. In addition, this study adopts scanning electron microscopy to characterize the worn surface.

#### 3. PERFORMANCE ANALYSIS OF NBC-NI/MLG METAL CERAMICS

NbC-Ni/MLG metal ceramics' mechanical and frictional wear properties were analyzed. This study analyzes how different sintering temperatures and MLG contents affect the Vickers hardness, fracture toughness, and bending strength of NbC-Ni/MLG. The study also conducts grain size and phase analysis. For the friction and wear properties of NbC-Ni/MLG metal ceramics, materials'

friction coefficient and wear amount under different hardness friction are analyzed and explained.

#### 3.1. Mechanical properties analysis of NbC-Ni/MLG metal ceramics

By preparing NbC-Ni/MLG metal ceramics at different sintering temperatures, materials with varying mechanical properties can be obtained. Under the sintering temperature schemes of B1, B2, B3, and B4, Fig. 2 shows the bending strength, Vickers hardness, and fracture toughness of NbC-Ni/MLG metal ceramics with five different MLG contents.

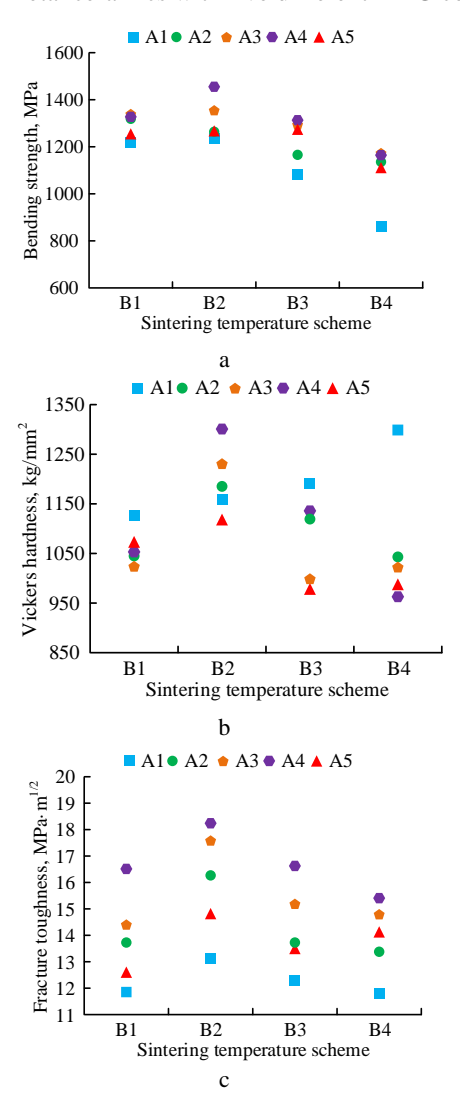


**Fig. 2.** NbC-Ni/MLG metal ceramics' mechanical properties at different sintering temperatures: a—bending strength; b—Vickers hardness; c—fracture toughness

In Fig. 2 a, as the sintering temperature increases, NbC-Ni/MLG metal ceramics' bending strength with different MLG contents first increases and then decreases overall. The inflection point of the trend change is 1440 °C. In addition, NbC-Ni/MLG metal ceramics' maximum bending strength with different MLG contents are 1238 MPa, 1313 MPa, 1358 MPa, 1456 MPa, and 1275 MPa, respectively. This indicates that NbC-Ni/MLG metal ceramics with different MLG contents have higher bending strength at a sintering temperature of 1440 °C. In Fig. 2 b, except for the case where the MLG content is 0, NbC-

Ni/MLG metal ceramics' maximum Vickers hardness at all other MLG contents occurs at 1440 °C. They are  $1180 \text{ kg/mm}^2$ ,  $1230 \text{ kg/mm}^2$ ,  $1300 \text{ kg/mm}^2$ , 1120 kg/mm<sup>2</sup>, respectively. In Fig. 2 c, the fracture toughness of NbC-Ni/MLG metal ceramics increases first and then decreases with the increase of sintering temperature under different MLG contents. NbC-Ni/MLG metal ceramics' maximum fracture toughness under different MLG amounts occur at 1440 °C. They are 13.01 MPa·m<sup>1/2</sup>, 16.25 MPa·m<sup>1/2</sup>, 17.58 MPa·m<sup>1/2</sup>, 18.24 MPa·m<sup>1/2</sup>, and 14.80 MPa·m<sup>1/2</sup>, respectively. In summary, NbC-Ni/MLG metal ceramics exhibit better mechanical properties when the sintering temperature is 1440 °C. Fig. 3 shows how the MLG content affects the mechanical properties and grain size of NbC-Ni/MLG metal ceramics.

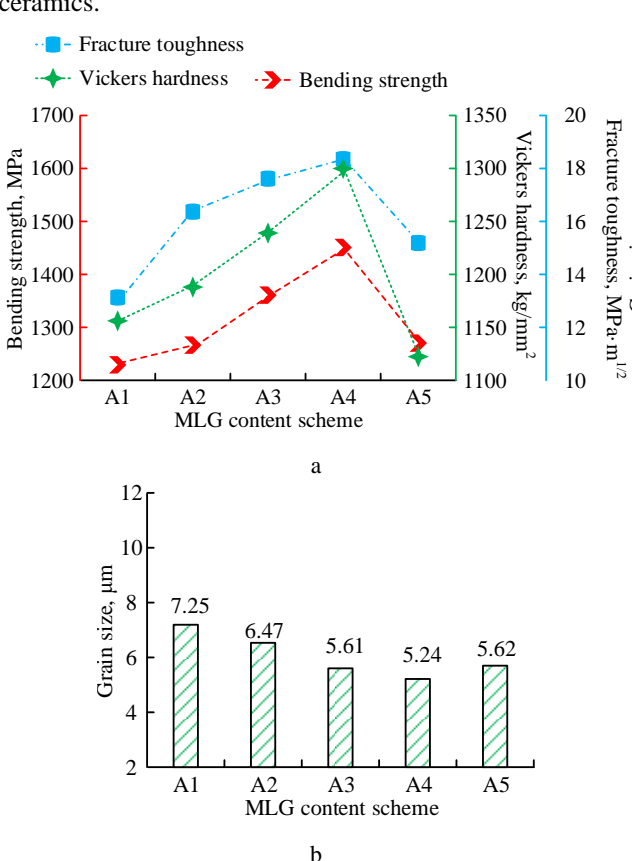


**Fig. 3.** MLG's effect on NbC-Ni/MLG metal ceramics' mechanical properties and grain size: a – mechanical property; b – grain size.

In Fig. 3 a, at a sintering temperature of 1440 °C, with the increasing MLG, the bending strength, Vickers hardness, and fracture toughness of NbC-Ni/MLG metal ceramics first increase and then decrease, with a turning point value of 0.75 wt.%. The maximum values of bending strength, Vickers hardness, and fracture toughness corresponding to different MLG contents are 1456 MPa, 1300 kg/mm², and 18.24 MPa·m¹/², respectively. The MLG content corresponding to these maximum values is 0.75 wt.%. This indicates that NbC-Ni/MLG metal ceramics have better mechanical properties when the MLG content is 0.75 wt.%. In Fig. 3 b, with the increase of MLG, NbC-Ni/MLG metal ceramic's grain size first gradually decreases and then increases. The maximum and minimum grain sizes

are 7.25  $\mu$ m and 5.24  $\mu$ m, respectively, with a difference of 2.01  $\mu$ m. The corresponding MLGs are 0 wt.% and 0.75 wt.%, respectively. The addition of MLG can reduce grain size and inhibit grain growth, but excessive MLG content will reduce the inhibitory effect. Fig. 4 shows MLG initial powder and NbC-Ni/MLG's XRD diffraction spectra.

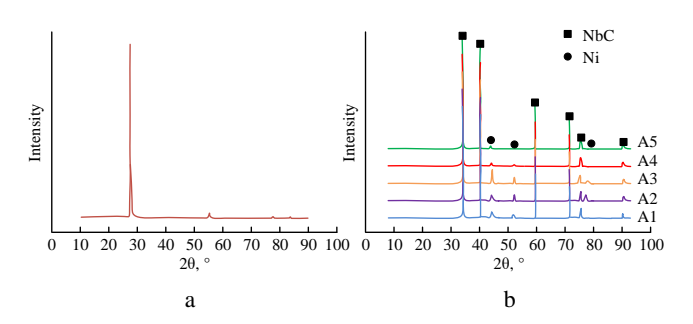


**Fig. 4.** XRD diffraction spectra: a – XRD diffraction spectrum of MLG initial powder; b – XRD diffraction spectra of NbC-Ni/MLG under different MLG content schemes

In Fig. 4 a, a distinct graphite crystal plane characteristic peak appears in the initial MLG powder's XRD diffraction spectrum, which is due to the stacked structure of MLG. In Fig. 4 b, NbC-Ni/MLG metal ceramics' XRD diffraction spectra with different MLG contents only show characteristic peaks of NbC and Ni, lacking characteristic peaks of other raw materials. This indicates that the introduction of MLG cannot lead to phase transition. In addition, compared with the XRD diffraction spectrum at 0 wt.% content, the XRD diffraction spectra at other MLG contents also lack significant graphene characteristic peaks. This is because graphene has a lower content and is more dispersed. Fig. 5 shows the Raman spectra of the initial powder, mixed powder, and sample under A4 scheme.

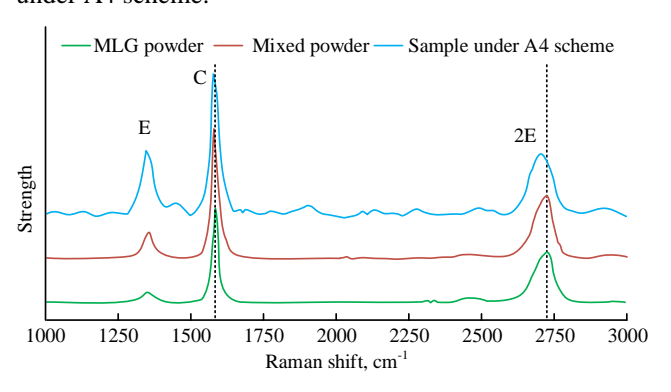


**Fig. 5.** Raman spectra of initial powder, mixed powder, and samples under A4 scheme

In Fig. 5, peak C represents graphene's main characteristic peak and mainly appears at a Raman shift of 1582 cm<sup>-1</sup>. In addition, both peaks E and 2E represent the disorder of graphene and appear at Raman shifts of 1360 cm<sup>-1</sup> and 2720 cm<sup>-1</sup>, respectively. In addition, peaks C and E's intensity ratio can explain the defect density of graphene. The initial powder, mixed powder, and A4 scheme samples' strength ratios are 0.13, 0.42, and 0.68, respectively. The mixed powder and A4 scheme samples' strength ratios are significantly higher than the initial powder's. This indicates that both high-energy ball milling

and high-temperature sintering can deepen graphene's defect density. In the sample under A4 scheme, both peaks C and 2E shift slightly to the left, indicating that graphene contains less tensile stress. Fig. 6 shows the fracture morphology of NbC-Ni/MLG under five different MLG schemes.

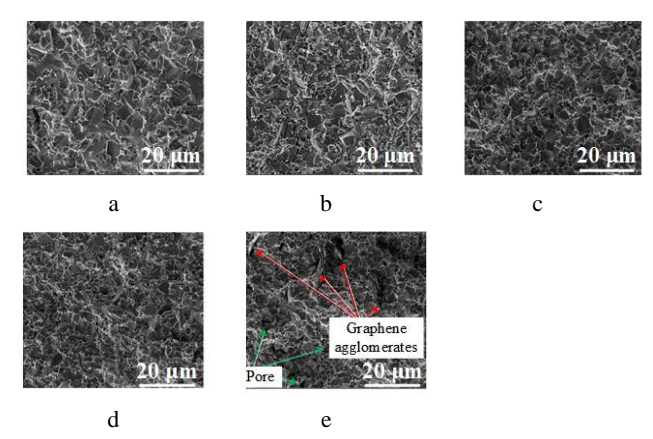


**Fig. 6.** Fracture morphology of NbC-Ni/MLG under five MLG schemes: a-A1; b-A2; c-A3; d-A4; e-A5

Fig. 6 show NbC-Ni/MLG's fracture morphology at 0 wt.%, 0.25 wt.%, 0.5 wt.%, 0.75 wt.%, and 1 wt.%, respectively. In Fig. 6 a, there are mainly two types of fracture morphology, namely transgranular fracture and transgranular fracture. In Fig. 6 b, c, d, and e, the proportion of transgranular fractures in the fracture morphology begins to increase when MLG is added. Furthermore, as MLG increases, the graphene agglomeration becomes more pronounced. When the MLG is 0.75 wt.%, the fracture morphology's grain size is smaller and more uniform. Fig. 7 shows TG-DSC under different MLG schemes.

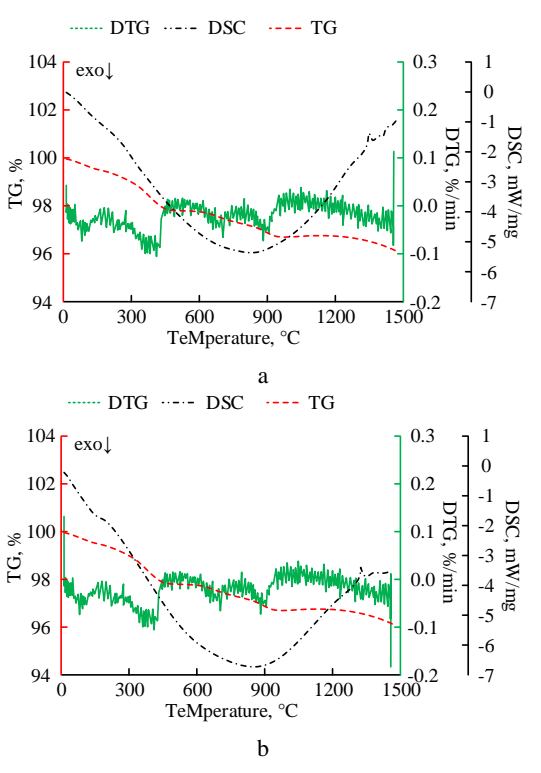
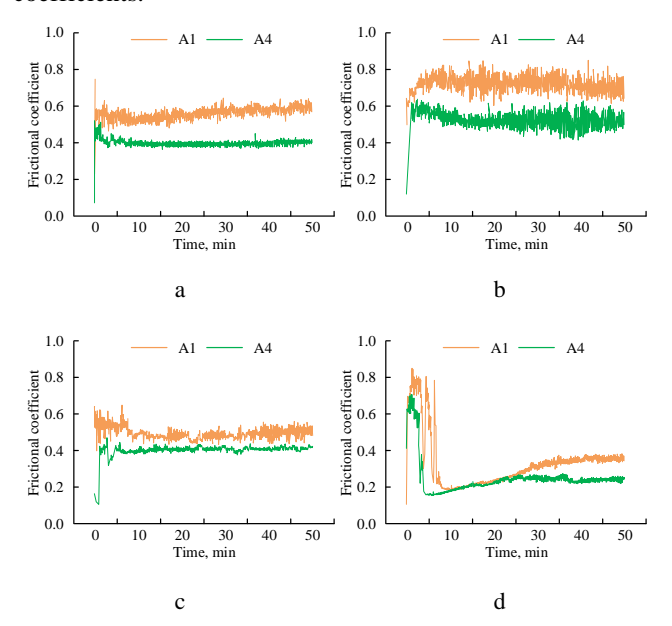


Fig. 7. TG-DSC results under different MLG schemes: a-TG-DSC results under A1 scheme; b-TG-DSC results under A4 scheme

In Fig. 7, exo represents the heat releasing direction. In Fig. 7 a, when MLG is 0 wt.%, TG has maximum and minimum values of 100 % and 96 %, respectively. DSC has maximum and minimum values of 0 mW/mg and -5.32 mW/mg, respectively. As the temperature increases, TG gradually decreases. DSC first decreases and then increases. In addition, Derivative Thermo Gravimetry (DTG) has maximum and minimum values of 0.122 %/min and -0.118 %/min, respectively. In Fig. 7 b, when MLG is 0.75 wt.%, TG remains basically unchanged. DSC has a maximum value of -0.25 mW/mg and a minimum value of -6.85 mW/mg, a decrease of 1.53 mW/mg. The maximum and minimum values of DTG are 0.135 %/min and -0.189 %/min, respectively. Overall, the combination of MLG and NbC-Ni is mechanical bonding.

### 3.2. Analysis of friction and wear properties of NbC-Ni/MLG metal ceramics

To analyze the friction and wear properties of NbC-Ni/MLG metal ceramics, the friction coefficient is obtained through a friction and wear testing machine. Grinding balls of different hardness have different friction coefficients. The study selects A1 and A4 schemes, with MLG contents of 0 wt.% and 0.75 wt.%, respectively. Figure 8 shows the two schemes and different grinding balls' friction coefficients.



**Fig. 8.** Friction coefficient between A1 and A4 schemes and different grinding balls: a – under the 304 stainless steel grinding ball; b – under the 45 steel grinding ball; c – under GCr15 steel; d – under YG6 hard alloy grinding ball

In Fig.8 a, under the grinding ball of 304 stainless steel, with the increase of friction time, the friction coefficient of the A1 scheme shows a fluctuating trend of rising and falling repeatedly. The friction coefficient under the A4 scheme first increases and then decreases and finally runs smoothly. The A1 and A4 schemes have maximum friction coefficients of 0.75 and 0.39, and minimum coefficients of 0.23 and 0.11, respectively. In Fig. 8 b, under the grinding ball of 45 steel, the friction coefficients of A1 and A4 schemes have been improved to a certain extent. Their corresponding maximum values are 0.84 and 0.64,

respectively. In Fig. 8 c and d, under the grinding ball of GCr15 steel and YG6 hard alloy, the friction coefficient of the A1 scheme is generally higher than the A4 scheme's. In summary, adding MLG can reduce the friction coefficient and improve the anti-friction effect of metal ceramics. Fig. 9 shows grinding balls' cross-sectional profiles of wear marks for the A1 scheme, A4 scheme, and different hardness.

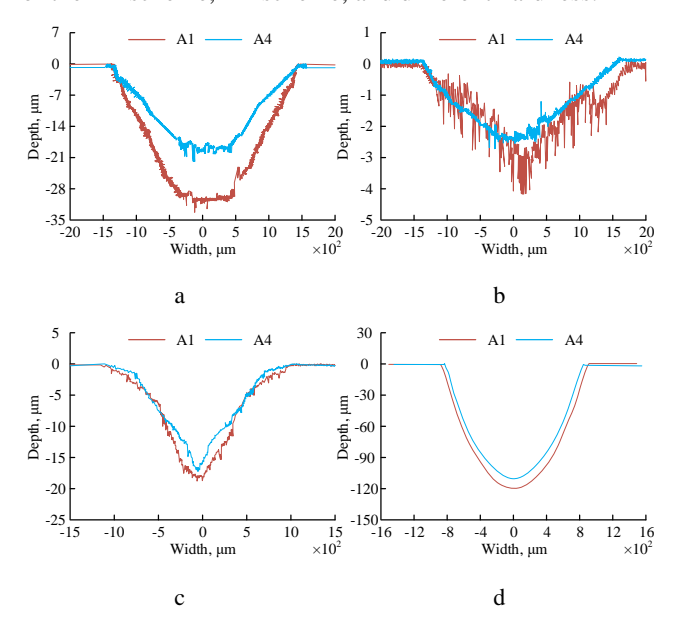


**Fig. 9.** The cross-sectional profile of wear marks between A1 and A4 schemes and grinding balls of different hardness: a – under the 304 stainless steel grinding ball; b – under the 45 steel grinding ball; c – under GCr15 steel; d – under YG6 hard alloy grinding ball

In Fig. 9 a, under the grinding ball of 304 stainless steel, the minimum depth of the grinding scratches corresponding to A1 and A4 schemes are -33.75 µm and -21.98 µm, respectively, with a significant difference of 11.77 µm. In addition, there is not much difference in the width of the wear marks between the two schemes. In Fig. 9 b, under the grinding ball of 45 steel, the grinding scratches' width and depth corresponding to A1 and A4 schemes are relatively close. The minimum depth of wear marks for the two schemes is -4.30 µm and -2.73 µm, respectively, with a difference of only 1.57 µm, which is significantly smaller than the 11.77 µm of 304 stainless steel under the grinding ball. In Fig. 9 c, under the grinding ball of GCr15 steel, the grinding scratches' width for the two schemes is consistent. The minimum grinding scratches' depth values are -18.76 μm and 17.1 μm, respectively, with little difference. In Fig. 9 d, there is a slight difference in the grinding scratches' width of these two schemes under the grinding ball of YG6 hard alloy. The maximum values are 1500 µm and 1560 µm, respectively. The minimum values are -1500 μm and -1440 μm, respectively. In addition, the two schemes have a minimum wear depth of -120 µm and -110 μm, respectively, with a difference of 10 μm. Overall, the A4 scheme, with an MLG content of 0.75 wt.%, has better mechanical properties and stronger resistance to deformation, rolling, and crushing. Fig. 10 shows the wear amount of grinding balls under different hardness for A1 and A4 schemes. In Fig. 10 a, under A1 scheme, these four hardness levels have corresponding wear amounts of

 $14.4 \times 10^{-6}$ ,  $1.327 \times 10^{-6}$ ,  $3.296 \times 10^{-6}$ , and  $34.59 \times 10^{-6}$  mm<sup>3</sup>/N·m for the grinding balls. YG6 hard alloy has the highest wear under the grinding ball, while 45 steel has the lowest wear under the grinding ball. In Fig. 10 b, under the A4 scheme, the corresponding wear amounts of the four hardness levels on the grinding balls are  $7.517 \times 10^{-6}$ ,  $0.9915 \times 10^{-6}$ ,  $2.682 \times 10^{-6}$ , and  $24.03 \times 10^{-6}$  mm<sup>3</sup>/N·m, respectively

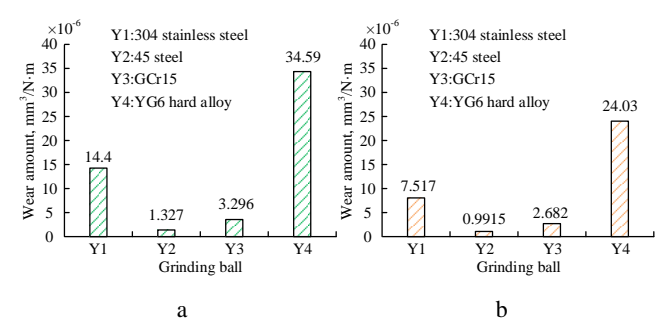
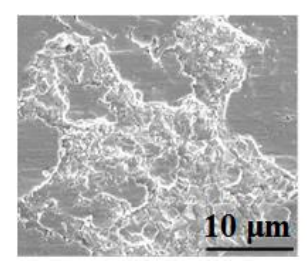
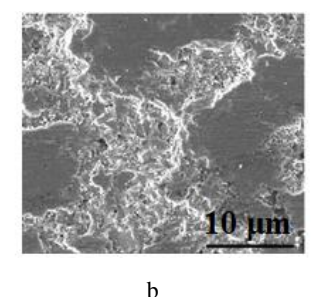


Fig. 10. The wear amount of A1 and A4 schemes under different hardness on grinding balls: a-under the A1 scheme; b-under the A4 scheme

These results are 6.883×10<sup>-6</sup>, 0.3355×10<sup>-6</sup>, 0.613×10<sup>-6</sup>, and 10.56×10<sup>-6</sup> mm³/N·m less than A1 scheme's, respectively. Therefore, the addition of MLG can enhance NbC-Ni metal ceramics' friction and wear performance, reduce wear, and promote the industrialization of Tujia jar tea using NbC-Ni/MLG as RTC material. Fig. 11 is the worn surface area's Scanning Electron Microscope (SEM) images under A1 and A4 schemes.





**Fig. 11.** SEM images of the worn surface area under A1 and A4 schemes: a – under scheme A1; b – under scheme A4

Fig. 11 shows the SEM image of the worn surface area under the grinding ball of 304 stainless steel. In Fig.11 a, under the A1 scheme without MLG, there are more attachments and debris on the surface of the grinding scratch. The debris distribution is relatively uniform. In addition, a small portion of metal ceramics are also exposed. In Fig. 11 b, after repeated friction on the sample under the A4 scheme, there are fewer debris left on the sample's grinding scratch surface. There are more exposed metal ceramics. In summary, MLG can reduce the friction between metal ceramics and grinding balls, lower the friction coefficient and wear amount, and promote the industrialization of Tujia jar tea using NbC-Ni/MLG as RTC material.

#### 4. DISCUSSION

In response to the issue of improving the mechanical and frictional wear properties of Tujia tea can materials, NbC Ni/MLG metal ceramic materials were studied and modified with different contents of MLG. The results showed that MLG can improve the mechanical and friction wear properties of NbC Ni/MLG metal ceramic materials, and the mechanical properties reached their optimum when the MLG content was 0.75 wt.%. In addition, after adding MLG, the wear amount of NbC Ni/MLG metal ceramic material decreased.

The introduction of MLG can enhance the performance of NbC-Ni metal ceramics, which is consistent with the research results of experts such as Wang Z. Experts such as Wang Z modified Ti (C, N) – based self-lubricating metal ceramics with different secondary carbides (NbC, tungsten carbide, tantalum carbide, and molybdenum carbide), achieving a reduction in friction coefficient and a delay in wear deterioration of the metal ceramics [20]. Carbides exhibit good performance in the modification of metal ceramics. Moustafa E B and other experts used three types of nano ceramic reinforcement particles, namely silicon carbide, aluminum oxide, and boron nitride, to improve the performance of NbC metal ceramics. The results showed that the static elastic modulus and compressive stress of NbC+SiC hybrid composite materials were increased by about 23.6 % and about 24 % respectively compared to the matrix alloy, and the comprehensive performance of NbC+SiC hybrid composite materials was better [21].

In early research, experts would enhance the performance of NbC metal ceramics by adding carbides, such as carbon monoxide [22]. Based on this tradition, MLG, which is also a carbide, was introduced into NbC-Ni metal ceramics to further enhance their performance. In addition, the research results can provide methodological support for future studies on improving the performance of NbC metal ceramics, as well as provide practical examples for the application of carbides in NbC metal ceramics and promote the development of carbides in the modification of metal ceramic materials.

#### 5. CONCLUSIONS

NbC-Ni/MLG metal ceramic materials are prepared, and their properties are analyzed. This can enhance Tujia jar tea RTC materials' mechanical and frictional wear properties, promoting the RTC industrialization. When the sintering temperature was 1440 °C, NbC-Ni/MLG metal ceramics with different MLG contents had maximum bending strengths of 1238 MPa, 1313 MPa, 1358 MPa, 1456 MPa, and 1275 MPa, respectively. The Vickers' hardness and fracture toughness both reached their maximum values. When MLG was 0.75 wt.%, the bending strength, Vickers hardness, and fracture toughness were the highest. The grain size of 5.24  $\mu m$  was the smallest.

In the XRD diffraction spectrum, the MLG characteristic peaks were missing, indicating that the introduction of MLG could not lead to phase transition. The initial powder, mixed powder, and A4 scheme samples had strength ratios of 0.13, 0.42, and 0.68, respectively. This indicated that both high-energy ball milling and high-temperature sintering could further deepen the defect density of graphene.

When MLG was 0.75 wt.%, TG, DSC, and DTG had minimum values of 96 %, -6.85 mW/mg, and -0.189 %/min,

respectively, indicating that the combination of MLG and NbC-Ni was mechanical. Under the four hardness grinding balls, the A1 scheme's friction coefficient was generally higher than the A4 schemes. Under the 304 stainless steel grinding ball, the grinding scratch's minimum depth corresponding to the A1 and the A4 schemes differed by 11.77  $\mu$ m. After adding 0.75 wt.% MLG, these four hardness levels' corresponding wear amounts on the grinding balls decreased by  $6.883 \times 10^{-6}$ ,  $0.3355 \times 10^{-6}$ ,  $0.613 \times 10^{-6}$ , and  $10.56 \times 10^{-6}$  mm³/N·m, respectively. Therefore, the addition of MLG can enhance NbC-Ni metal ceramics' friction and wear performance and reduce the wear amount.

There are also certain shortcomings in the research. Firstly, the research on the application of graphene materials is relatively simple. Future research can combine it with other carbides to enhance its performance. Secondly, the dispersion effect of graphene in metal ceramics needs to be optimized. Future research can focus on this to enhance the mechanical properties of materials. Thirdly, the study mainly analyzed the mechanical properties and friction and wear properties of NbC Ni/MLG metal ceramic materials, with less consideration given to the material's heat resistance and drop resistance. Future research can comprehensively consider the properties of materials from multiple perspectives to enhance their overall performance.

#### REFERENCES

- Lin, S., Chen, Z., Chen, T., Deng, W., Wan, X., Zhang, Z. Theanine Metabolism and Transport in Tea Plants (Camellia sinensis L.): Advances and Perspectives *Critical Reviews in Biotechnology* 43 (3) 2022: pp. 327 – 341. https://doi.org/10.1080/07388551.2022.2036692
- Zhang, X., Du, X., Li, Y., Nie, C., Wang, C., Bian, J., Luo, F. Are Organic Acids Really Related to the Sour Taste Difference between Chinese Black Tea and Green Tea? Food Science & Nutrition 10 (6) 2022: pp. 2071 – 2081. https://doi.org/10.1002/fsn3.2823
- Sun, L., Zhou, J.L., Cai, Q., Liu, S., Xiao, J. Comparing Surface Erosion Processes in Four Soils from the Loess Plateau under Extreme Rainfall Events International Soil and Water Conservation Research 9 (4) 2021: pp. 520-531. https://doi.org/10.1016/j.iswcr.2021.06.008
- 4. **Jose, S.A., John, M., Menezes, P.L.** Cermet Systems: Synthesis, Properties, and Applications *Ceramics* 5 (2) 2022: pp. 210–236. https://doi.org/10.3390/ceramics5020018
- Guo, M., Dong, Q., Xie, H., Wang, C., Zhao, Y., Wang, X., Zhong, W., Li, Z., Wang, R., Wang, Y., Hao, L., He, S., Chen, G., Xiong, W., Zhao, J.C., Hu, L. Ultrafast High-temperature Sintering to Avoid Metal Loss toward High-performance and Scalable Cermets Matter 5 (2) 2022: pp. 594 604. https://doi.org/10.1016/j.matt.2021.11.008
- Xiong, H., Xie, D., Chen, J., Chu, S., Gan, X., Li, Z., Zhou, K. Ti(C,N)-based Cermets with Strengthened Interfaces: Roles of Secondary Cubic Carbides *Journal of the American Ceramic Society* 103 (3) 2019: pp. 1582 1592. https://doi.org/10.1111/jace.16893
- Huang, J., Huang, S., Vleugels, J. Effect of Carbon and Tungsten Content on the Phase Equilibria, Microstructure,

- and Mechanical Properties of (Nb,W)C–Ni Cermets *Journal* of the American Ceramic Society 106 (7) 2023: pp. 4455–4468. https://doi.org/10.1111/jace.19069
- Fernandes, L.J., Stoeterau, R.L., Batalha, G.F., Rodrigues, D., Borrile, A.V. Wear Analysis of NbC-Ni Cemented Carbides for Cutting Tools Advances in Materials and Processing Technologies 8 (1) 2020: pp. 305 321. https://doi.org/10.1080/2374068x.2020.1808925
- 9. **Hübler, D., Gradt, T.** Effect of Different Binders and Secondary Carbides on NbC Cermets Forschung Im Ingenieurwesen 86 (2) 2022: pp. 197–211. https://doi.org/10.1007/s10010-022-00583-1
- Liu, X., Peng, Y., Zhou, P., Guan, Y., Mao, H., Kong, Y., Du, Y. Diffusion Behavior of Secondary Carbides and Subsequent Influence on Microstructure of NbC-Ni-Based Cermets *Journal of Phase Equilibria and Diffusion* 44 (1) 2023: pp. 150–162. https://doi.org/10.1007/s11669-023-01027-1
- Lin, F., Du, Y., Lv, J., Zhang, C., Liu, X., Tan, Z. Effect of NbC on the Microstructure, Mechanical Properties, and Oxidation Resistance of Ti(C,N)-based Cermets International Journal of Materials Research 111 (6) 2020: pp. 479 – 490. https://doi.org/10.3139/146.111907
- 12. Tang, S., Zhang, H., Yang, Z., Liu, Q., Lv, Z., Ouyang, C., Qiu, X. Microstructure and Mechanical Properties of NbC–Ni Cermets Prepared by Microwave Sintering High Temperature Materials and Processes 41 (1) 2022: pp. 482 492. https://doi.org/10.1515/htmp-2022-0049
- 13. **Ren, T., Wang, X., Wang, N., Huang, D., Zhu, Y., Shen, P.K., Zhu, J.** Regulating the Interfacial Electric Field of NbP–NbC Heterostructures to Efficiently Inhibit Polysulfide Shuttling in Li–S Batteries *Journal of Materials Chemistry A* 12 (9) 2024: pp. 5307–5318. https://doi.org/10.1039/d3ta07510a
- 14. Li, Q., Ling, Y., Zheng, H., Chen, G., Chen, J., Koppala, S., Jiang, Q., Li, K., Omran, M., Gao, L. Phase Microstructure and Morphology Evolution of MgO-PSZ Ceramics during the Microwave Sintering Process Ceramics International 47 (11) 2021: pp. 15849 15858. https://doi.org/10.1016/j.ceramint.2021.02.159
- 15. Basit, A., Anwar, F., Ali, S., Umer, M.A., Shahbaz, T., Din, E.U., Mubashar, A. Fe-Ni Binder Modified NbC Cermets: A Cost-effective Solution with Superior Mechanical Properties *Ceramics International* 50 (22) 2024: pp. 47768 47779. https://doi.org/10.1016/j.ceramint.2024.09.121
- 16. Chudoba, T., Griepentrog, M. Comparison between Conventional Vickers Hardness and Indentation Hardness Obtained with Different Instruments Zeitschrift Für Metallkunde 96 (11) 2005: pp. 1242 – 1246. https://doi.org/10.3139/146.101168
- Mousavi, S.R., Estaji, S., Paydayesh, A., Arjmand, M., Jafari, S.H., Nouranian, S., Khonakdar, H.A. A Review of Recent Progress in Improving the Fracture Toughness of Epoxy-based Composites Using Carbonaceous Nanofillers *Polymer Composites* 43 (4) 2022: pp. 1871–1886. https://doi.org/10.1002/pc.26518
- 18. **Djafar, Z., Renreng, I., Jannah, M.** Tensile and Bending Strength Analysis of Ramie Fiber and Woven Ramie Reinforced Epoxy Composite *Journal of Natural Fibers* 18 (12) 2020: pp. 2315–2326. https://doi.org/10.1080/15440478.2020.1726242

- Tabrizi, A.T., Aghajani, H., Laleh, F.F. Tribological Study of Thin-Electroplated Chromium: Evaluation of Wear Rate as a Function of Surface Roughness *Experimental Techniques* 47 (2) 2021: pp. 369 379. https://doi.org/10.1007/s40799-021-00502-z
- Wang, Z., Wan, W., Wang, J., Fan, K., Li, Y., Xiong, J., Du, H. Carburization and Wear Behavior of Self-lubricating Ti (C, N)-based Cermets with Various Secondary Carbides *Ceramics International* 47 (19) 2021: pp. 26678 26691. https://doi.org/10.1016/j.ceramint.2021.06.075
- Moustafa, E.B., Abushanab, W.S., Ghandourah, E.I.,
  Taha, M.A., Mosleh, A.O. Advancements in Surface
- Reinforcement of AA2024 Alloy Using Hybridized Niobium Carbide and Ceramics Particles via FSP Technique *Metals and Materials International* 30 (3) 2024: pp. 800 813. https://doi.org/10.1007/s12540-023-01541-4
- 22. Okovity, V.A., Panteleenko, F.I., Okovity, V.V., Astashinsky, V.M. Formation of Plasma Powder Coatings from Cermet with Subsequent High-Energy Modification Science & Technique 19 (6) 2020: pp. 469 474. https://doi.org/10.21122/2227-1031-2020-19-6-469-474



© Shi et al. 2025 Open Access This article is distributed under the terms of the Creative Commons Attribution 4.0 International License (http://creativecommons.org/licenses/by/4.0/), which permits unrestricted use, distribution, and reproduction in any medium, provided you give appropriate credit to the original author(s) and the source, provide a link to the Creative Commons license, and indicate if changes were made.